Progress In Electromagnetics Research, Vol. 149, 147–160, 2014

A Design of Multiband, Dual-Polarization, Beam-Switchable Dual-Antenna for Indoor Base Stations

Viet-Anh Nguyen*, Rao Shahid Aziz, Seong-Ook Park, and Giwan Yoon

Abstract—A novel multiband, dual-polarization, beam-switched dual-antenna design, covering some LTE and WLAN bands, has been proposed for indoor base stations. The proposed design consists mainly of dual modified monopole antennas. The horizontal antenna consists of four printed monopole elements, and the control circuit using p-i-n diodes has been implemented for feeding to each monopole element. The vertical monopole antenna beam patterns are controlled by reconfigurable frequency selective reflectors (RFSR) technique. The p-i-n diodes have been utilized for switching mechanism to feed the four RFSR. The measured and simulated results indicate that the antenna system possesses multiband and dual polarization. It has been observed from the simulated and measured reflection coefficients $|S_{11}|$ that the presented dual antenna system supports both LTE (1.7–2.1 GHz) and WLAN (2.5 GHz and 5.8 GHz) band frequencies. Moreover, the radiation characteristics show dual-polarization behaviors of the presented antenna system and beam switching states suitable for small cell indoor-base stations.

1. INTRODUCTION

Immense growth in the communication technologies has increased the demand for small indoor base stations and also the need for multi-functional wireless communications in a single device. Over the last two decades, the dramatic development of the base station antenna technology has been made. Currently, the requirements in the antenna technology include dual-polarization, omnidirectional radiation pattern diversity and high channel capacity when all-the-direction communication is requisite. Dual polarized antennas possess vertical as well as horizontal polarizations. When the said polarizations show orthogonal radiation patterns, they lead to achieving high capacity in rich multipath environments. The pattern diversity can be obtained by the application of different antennas with different radiation patterns. Hence, different antennas with a beam switching scheme can be utilized on base station antennas for pattern diversity. Many dual polarization and pattern diversity antennas for cellular base station have been reported in [1–8]. In [5], Wang et al. proposed a pair of small and low-profile orthogonal dual-polarization combined antenna for a miniature indoor MIMO base station. In their antenna configurations, the vertical and horizontal polarizations were obtained by using both a disk-loaded monopole antenna and a notch array antenna with parasitic elements. Both antennas operate at the 2 GHz band of IMT-2000. A novel dual-band, broadband array antenna with low profile and dual polarization was presented by Liu et al. [6]. They used both arc-probe-fed annular ring elements and pairs of nested crossmicrostrip dipoles for the design of their array antenna. The measured impedance bandwidths were determined by the VSWR < 2 criterion, which covers 806–960 MHz and 1710–2170 MHz. Likewise in many other studies, the dual polarization was achieved by the combination of printed dipoles, patch elements arrays and spiral antennas, as reported in [1–4]. The pattern diversity approach was investigated by Tarn et al. in [9, 10]. Their study proposed a radiation pattern diversity

Received 31 July 2014, Accepted 30 September 2014, Scheduled 14 October 2014

* Corresponding author: Viet-Anh Nguyen (ngvanh78@kaist.ac.kr).

The authors are with the KAIST (Korea Advanced Institute of Science and Technology), 291 Daehak-ro, Yuseong-gu, Daejeon 305-701, Republic of Korea.

reflector antenna fed by a monopole. Moreover, they designed and developed novel switchable frequency selective reflectors to construct a square corner reflector antenna.

In this paper, we present a design of multiband, dual-polarization, beam switched dual-antenna system module suitable for small cell indoor base stations. The proposed antenna scheme is composed of both horizontal and vertical antennas on a single multi-layers substrate. The horizontal antenna consists of four monopoles for the radiation pattern diversity. A bias-switching circuit is designed to feed the four elements, using the BAR 64-02W [8] p-i-n diodes for the beam switching purpose. On the other hand, the vertical antenna consists of printed monopole in which the beam switching mechanism is achieved by the employment of reconfigurable frequency selective reflectors (RFSR) [10]. The vertical monopole antenna is surrounded by the RFSR feeding, based on the BAR 64-02W p-i-n diode switches. As a result of measurement, the proposed antenna scheme is found to cover LTE (1.7–2.1 GHz) and WLAN (2.4–2.5 GHz, 5.2 GHz and 5.8 GHz) standard bands with reasonably good bandwidths.

2. PROPOSED ANTENNA DESIGN CONCEPT

2.1. Antenna System Design and Configuration

The proposed multiband, dual-polarization dual-antenna system is fabricated on a single main multi-layer PCB board, which is made on an FR4 substrate of the relative permittivity $\varepsilon_r = 4.6$ and loss tangent $\tan\delta = 0.025$. The proposed dual antennas are mounted on the top of a main ground plane, which occupies a volume of $170 \times 150 \times 6\,\text{mm}^3$ suitable for small cell mobile/wireless indoor systems. A copper sheet of 0.2 mm thickness is used for the fabrication of the prototype antenna. In order to minimize the feed cable issues, the antenna is fed through an SMA connector placed at the bottom side of the ground plane. Figure 1 depicts the geometry view of the proposed antenna. As can be seen in Figure 1, it consists of two major parts: the horizontal antenna with four monopole printed

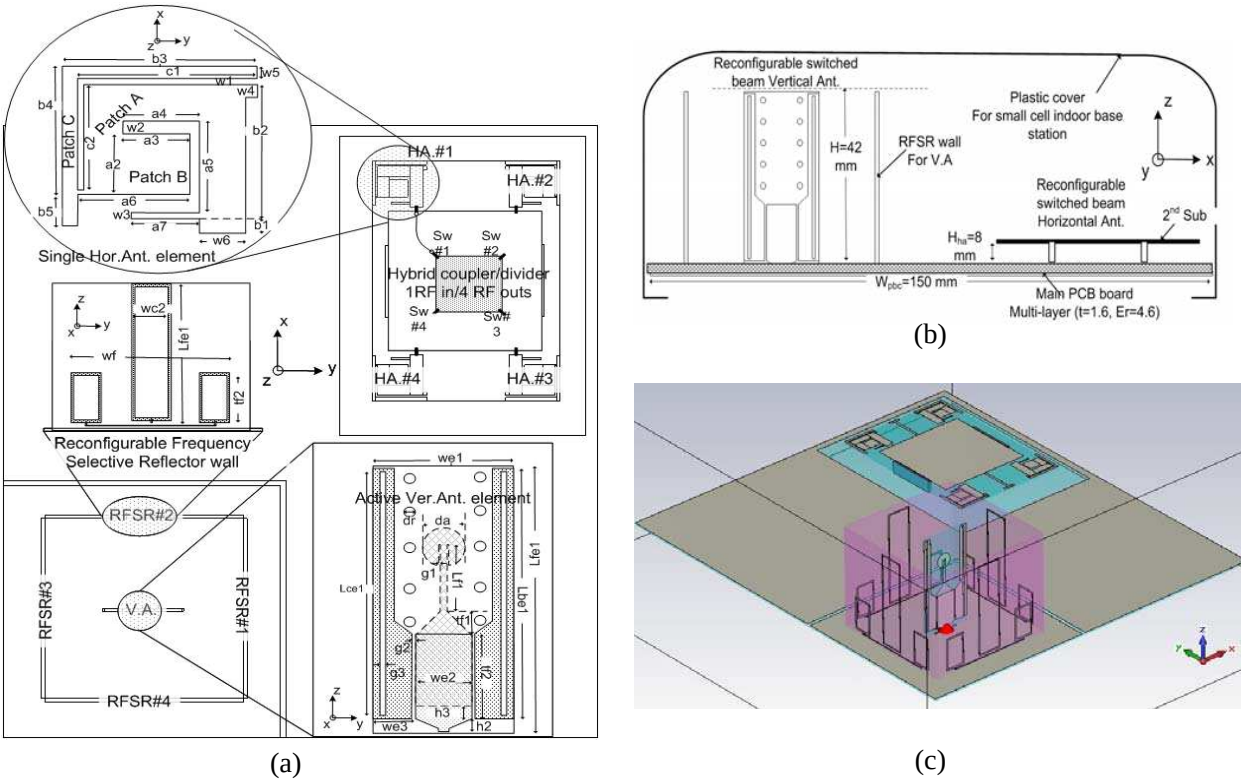

Figure 1. Proposed antenna configurations and dimensions. (a) Top-view with zoom-in antenna element; (b) side view; and (c) simulated CST 3D-view.

elements placed at each side of the substrate with p-i-n diode feeding switches and vertical monopole antenna encircled by four RFSR wall. The side-view and simulation based CST 3D-view of the proposed antenna configuration are shown in Figures 1(b) and (c), respectively. The presented dual antennas can be operated independently for both horizontal and vertical polarizations. In addition, the vertical antenna can be operated in two modes: omni-directional or beamswitchable modes. In contrast, the horizontal antenna, can only be utilized in switched-mode for desired direction. The whole antenna design supports the LTE (1.7–2.1 GHz) and WLAN (2.5 GHz and 5.8 GHz) band frequencies. The commercial EM full-wave simulator CST2009 program [11] was used to simulate and optimize the antenna parameters. Optimized dimensions of the complete antenna structure are given in Table 1.

2.2. Vertical Antenna Element Design

The vertical antenna element (V.A) is a printed monopole type, which is designed on an FR4-substrate (height = 0.8 mm, $\varepsilon_r = 4.6$, loss tangent = 0.025) and functions as an active radiating element. The V.A has a total size of $30 \times 10 \times 0.8\,\text{mm}^3$, which is mounted on the top of a sub-ground square size $70 \times 70\,\text{mm}^2$ of the main PCB. Figure 2 shows the optimized geometry dimensions and the notation of each patch of V.A. In order to make the V.A operate in switched modes, four reconfigurable frequency selective reflectors (RFSR) need to be placed around the active V.A with the optimization spacing of 25 mm far from the center [9, 10]. The RFSR is made of a Teflon substrate with $\varepsilon_r = 2.2$ and thickness of $t = 0.508$ mm. The RFSR is designed based on the common concept that when the length of the parasitic element is shorter than that of the active element, a pulling pattern is obtained. While, if the length of the parasitic element is longer than the active element, a pushing pattern is formed. Figures 3(a)–(c) show the parametric results of the V.A in this study. The black dash-dot line in Figure 3(a) indicates the scattering parameters of the vertical antenna when the patch A is applied

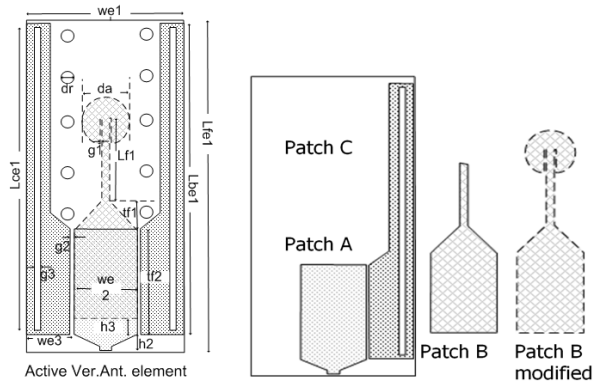

Parameter	VALUE	Parameter	VALUE	Parameter	VALUE
dr	1.4	tf1	3.75	b4	9.785
da	3	tf2	13.25	b5	2.375
Lce1	38	Lf1	10.5	c1	11.4
Lbe1	39	h2	2	c2	8.36
Lfe1	40	h3	1.515	a2	4.75
we2	8	wf	40	a3	4.75
we3	5.5	wc2	6	a4	5.225
g1	0.2	b1	1	a5	7.125
g2	0.5	b2	11.5	a6	8.075
g3	0.75	b3	12.825	a7	4.75
w1	0.525	w2	0.95	w6	3.325

Figure 2. The proposed vertical antenna geometry dimensions and its patch notation.

Table 1. Detailed parameters of the proposed antenna system in Figure 1(a).

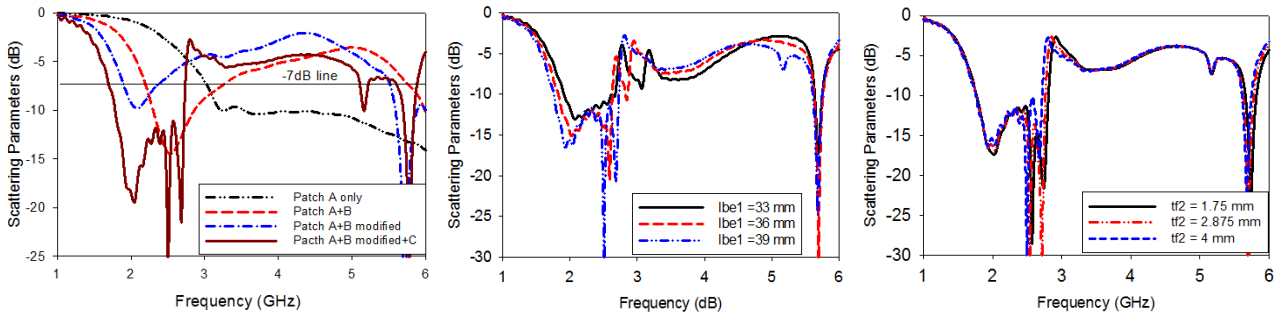

Figure 3. The simulated parametric study of the V.A antenna.

only. By putting another parasitic patch B and/or patch B modified on the bottom of the substrate which is 2 mm above from patch A, the antenna resonates on dual bands (the red dash line and blue dash-dot-dot line, respectively). Then, by adding the parasitic patch C in the left and right sides of the patch A, the antenna generates multiband operating frequencies (the dark red line in Figure 3(a)). Then, the Figures 3(b)–(c) show the change in scattering parameters when the parameters '*Lbe1*' and '*tf2*' vary, respectively. These parameters were optimized by the CST program. The simulated surface current distributions of the V.A at 1.75 GHz, 1.9 GHz, 2.5 GHz, and 5.8 GHz, respectively, are shown in Figure A1 of Appendix (Figure A1(a)). The total height of patch C, B and patch A is about 40 (*Lfe1*), 29 (*da/2* + *Lf1* + *tf1* + *tf2*), and 13.25 (*tf2*), which are approximation of $\lambda_g/4$ of the fundamental frequencies, respectively. Moreover by adding the parasitic of patch C both left and right side of patch A make the V.A become a broaden band at the lower frequency due to the coupling effects.

2.3. Horizontal Antenna Element Design

Similarly, the horizontal antenna element (H.A) is composed of four printed type monopoles placed on the top of the four corners of the 2nd sub-substrate. The ground with size of $38\times38\,\text{mm}^2$ of the horizontal antenna is placed at the bottom of the 2nd sub-substrate. The H.A is designed on an FR4-substrate ($\varepsilon_r = 4.6$ and thickness, $t = 1.2\,\text{mm}$). The total size of the H.A is $66.5 \times 47.5 \times 1.2\,\text{mm}^3$ mounted on top of the main PCB rectangular size $62 \times 83\,\text{mm}^2$ with the height of $h = 8\,\text{mm}$. The geometry and the notation of each antenna element of the H.A are shown in Figure 1. Figures 4(a)–(c) show the parametric study of the H.A where the parameters were also optimized by using the CST program in order to match the designed target resonant frequencies of the V.A reported in the previous section. The dark dash-dot line in Figure 4(a) indicates the scattering parameters of the H.A when only a monopole is applied. It can be seen that the H.A is operating at 2.8 GHz. In order to make the H.A have a multibands and match to the V.A, the patches A, B and C are created to tune up additional frequency bands. Finally, after the addition of the patches, the H.A also covers desired standard bands LTE (1.7–2.1 GHz) and WLAN (2.5 GHz and 5.8 GHz) with reasonable matching, as depicted in Figure 4. The final optimized values for the parameters c_2 and a_3 are illustrated in Figures 4(b)–(c), and their corresponding values are reported in Table 1. In order to further explain the horizontal antenna parts for achieving the multiband performances, the surface currents on the complete antenna structure for different frequencies are shown in Appendix Figure A1(b) at 1.75 GHz, 1.9 GHz, 2.5 GHz, and 5.8 GHz operating frequencies. To make compact volume size of H.A, the monopole patches are bended and take the advantages of mutal coupling effects. The corresponding physical length of H.A at the fundamental frequecies is about 41.085 ($47.5/2 - b_3 + b_4 + b_5 + 18$), 31.26 ($b_2 + c_1 + c_2$), and 12.35 ($a_3 + a_4$), which are also an approximation of $\lambda_g/4$ of the fundamental frequencies, respectively. (*The T-arm length of the T-shape in H.A is 18 mm.*).

2.4. The Feed and Control Networks

The proposed multiband, dual-polarization, dual-antenna is composed of V.A and H.A, both of which work in independent modes. The V.A and H.A were fed by two SMA-50 Ω ports underneath of the main substrate, respectively. The two antenna elements are placed at the two cross-corners of the main PCB,

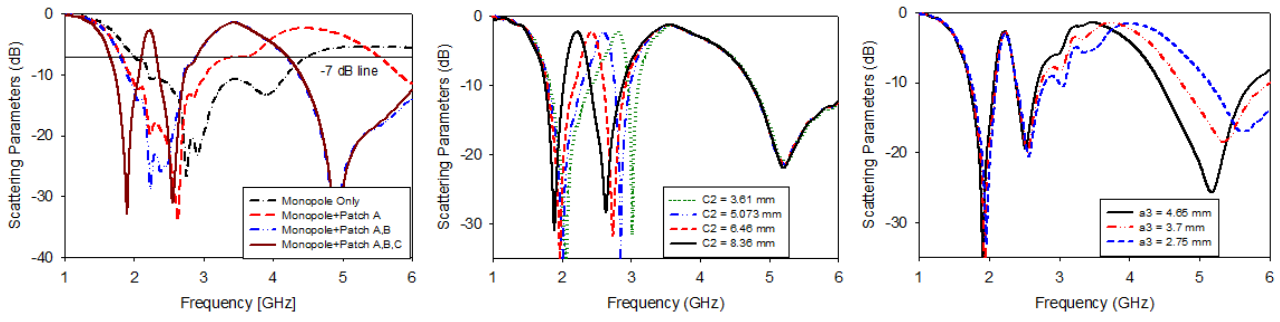

Figure 4. The simulated parametric study of the H.A antenna.

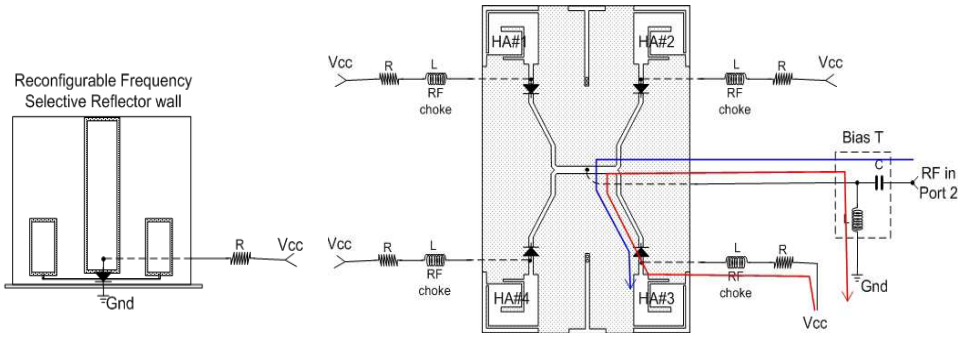

Figure 5. The proposed control circuits for V.A and H.A to control the beams ($R = 220\,\Omega$, $L = 1.82\,\text{nH}$, $C = 3.75\,\text{pF}$).

which are about 40 mm far from each other, guaranteeing a better isolation between the two ports. Making it possible that both V.A and H.A work independently requires the different control switches network for feeding. The V.A can work in two different modes: one is omni-direction mode, all p-i-n diode switches are OFF, while the other mode is directional mode in which one of RFSR#i (e.g., $i = 1$, 2, 3, 4) is activated for pulling or pushing the beam pattern in the desired direction of signals [2]. On the other hand, the H.A can only work in directional mode, which depends on the requirement which horizontal element (H.A#i) needs to be activated based on the incoming signals by controlling the p-i-n diode switches (Sw#i). In order to control the beam direction in the V.A, a simple control switch is applied for choosing the specific RFSR#i, which is activated by shorting it to the ground or deactivated by not shorting it, as shown in Figure 5(a). Similarly, the H.A antenna control circuit is proposed in Figure 5(b), where four sub-ports for input voltage (Vcc) supply are used to control the ON and OFF states of the implemented p-i-n diode switches (Sw#i) on each element of the H.A#i. To make a simple control circuit, a common ground is used for all switching ports, which makes it necessary to adopt a bias-T as an RF-input port. From Figure 5(b) it is noted that the red line indicates the Vcc-path loop of the current to control the SW#3 in activated mode, which will activate the H.A#3 of the horizontal antenna which functions as a radiator, while the blue line implies the RF-path to the H.A#3.

3. EXPERIMENTAL AND SIMULATED RESULTS

The commercial EM full-wave simulator CST2009 program was used to simulate and optimize the whole antenna parameters [11]. To validate the performance of the proposed antenna system, several samples of the vertical and horizontal antenna elements are fabricated. Figure 6 shows the prototype of the proposed antenna fabricated using the optimized parameters given in Table 1. The antenna system was fed by using coaxial cables through two SMA-50 Ω ports for V.A and H.A, separately. The reflection coefficients $|S_{11}|$ were measured by the Agilent-HP E8357A network analyzer, and the antenna radiation patterns were measured in an anechoic chamber with the size of $10\,\text{m}(L) \times 5\,\text{m}(H) \times 6\,\text{m}(W)$ located

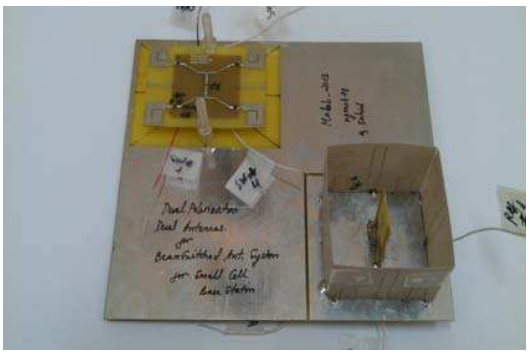

Figure 6. The prototype antenna fabricated with control circuits.

at KAIST. The performances of the return losses, gains, and radiation patterns were measured and compared to the simulation data results. In practical design of a base station antenna, a VSWR < 1.6 is required; however, for a research progress -7 dB reflection coefficient is acceptable since it does not contain a matching circuit. In this study, we use -7 dB line as a reference to evaluate the antenna performance.

As outlined in antenna system design and configuration section, the V.A antenna is operated in two modes, i.e., omnidirectional mode and beam switched mode. Figure 7(a) shows the 3D and 2D polar radiation patterns, obtained in omni-directional mode operation, of the V.A at xy, yz and xz-planes, respectively. In this mode, the beam patterns are almost omnidirectional with the maximum directivity gain of about 3.19 dBi with 30° on the elevation plane. In additional, the beam switched mode, only one RFSR#i among the four is activated [2]. As a result, the V.A beam patterns contain the maximum directivity gain in one direction, which is opposite to the activated RFSR#i due to the pressing or pulling pattern of the RFSR#i, as shown in Figure 7(b). In switched modes, the maximum directivity gain reaches 7.4 dBi, where the main lobe is about 5 dBi and the side lobe is -8.73 dBi.

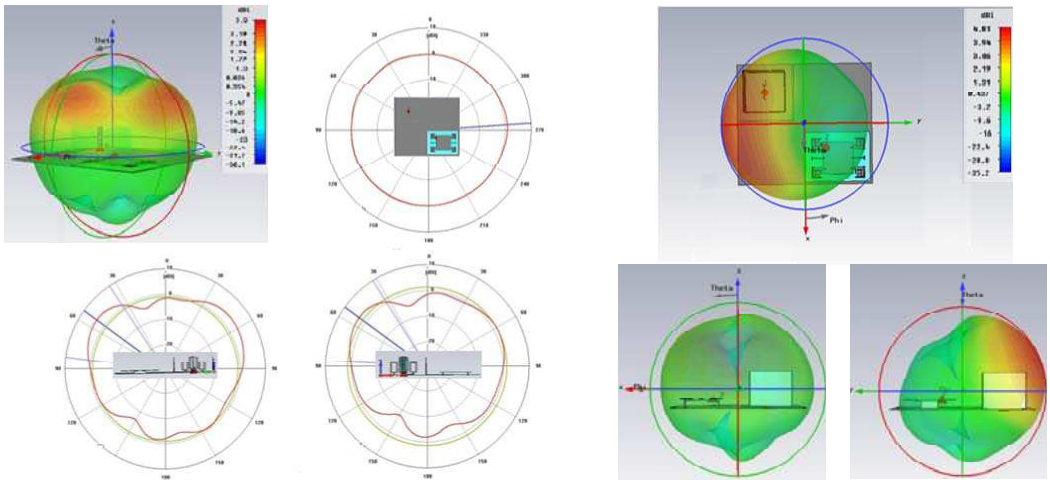

Figure 7. The simulated beam patterns of the V.A at 1.9 GHz. (a) Omni-directional mode, (b) switched mode.

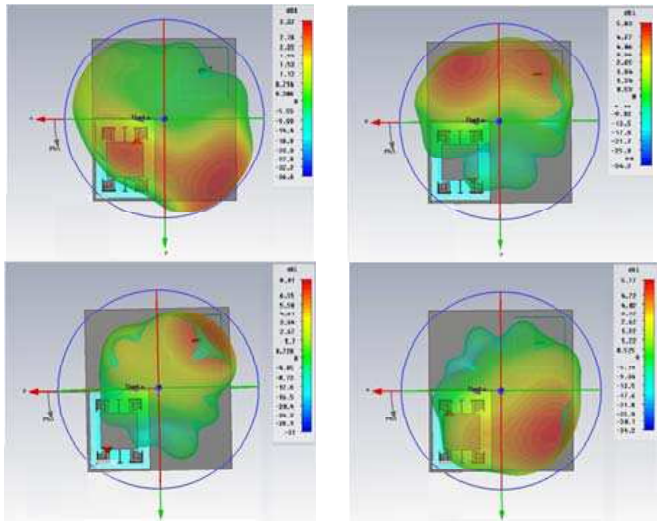

Figure 8. The simulated beam patterns of the H.A at 1.9 GHz in different switched modes.

In contrast, the H.A operates only in switched modes as previously discussed, and thus the beam patterns depend mainly on which H.A#i is selected for radiation. Figure 8 shows the beam patterns of the H.A, depending on the activation of the specific Sw#i. Figure 9 demonstrates the simulation (a) and measurement (b) S-parameters of the proposed multi-band, dual-polarization dual-antenna system. It is evident that both results are well matched at all the target frequencies of interest for the LTE (1.7–2.1 GHz) and WLAN (2.5 GHz and 5.8 GHz). As mentioned earlier, the two antenna elements can work independently with a reasonable isolation of −25 dB, and the beam patterns of each antenna can be controlled separately. Moreover, it was found that by utilizing the proposed antenna with switching mechanism, several different beam schemes could be achieved. In order to indicate the pattern behaviors, different beam controlled illustrations for V.A and H.A could be identified, as shown in Figure 10. As shown in the Appendix, from Figure A2 to Figure A4, the beam patterns of the V.A antenna, investigated in an anechoic chamber, are demonstrated for more study. Figure A2 shows the V.A antenna operation in omni-directional modes. Figure A3 and Figure A4 illustrate the V.A antenna operation in switched modes at 1.75 GHz and 5.8 GHz, respectively, where the RFSR#i is subsequently selected as an activated parasitic element. Similarly, the beam patterns of the H.A are studied, as shown in Appendix A from Figure A5 to Figure A8. The beam patterns of the H.A antenna, operating

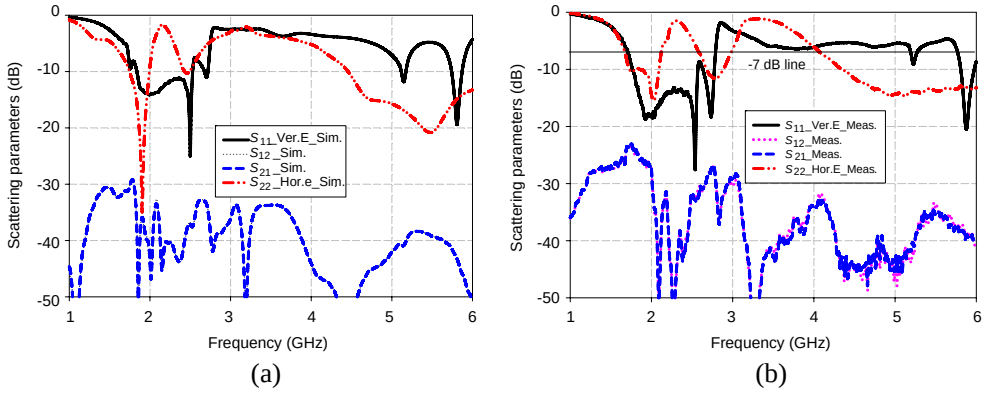

Figure 9. The comparison of (a) the simulated and (b) measured scattering parameters of the proposed antenna system.

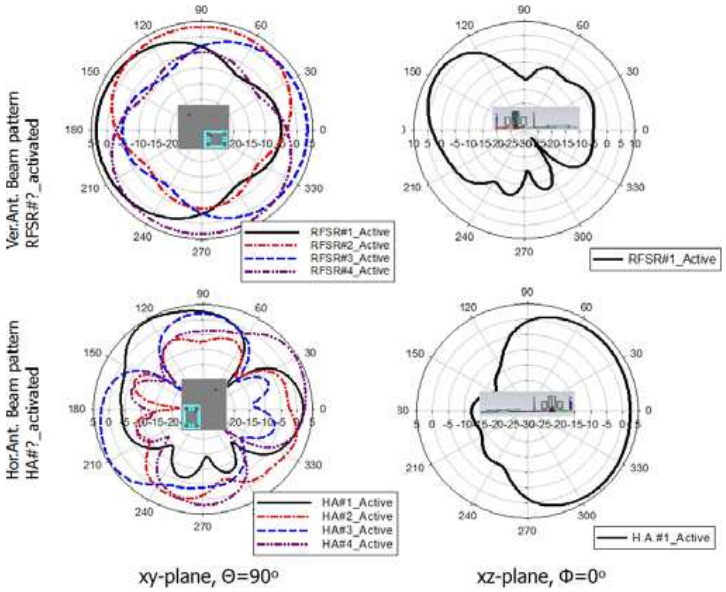

Figure 10. The demonstration of beam control treatments for V.A and H.A at 1.9 GHz.

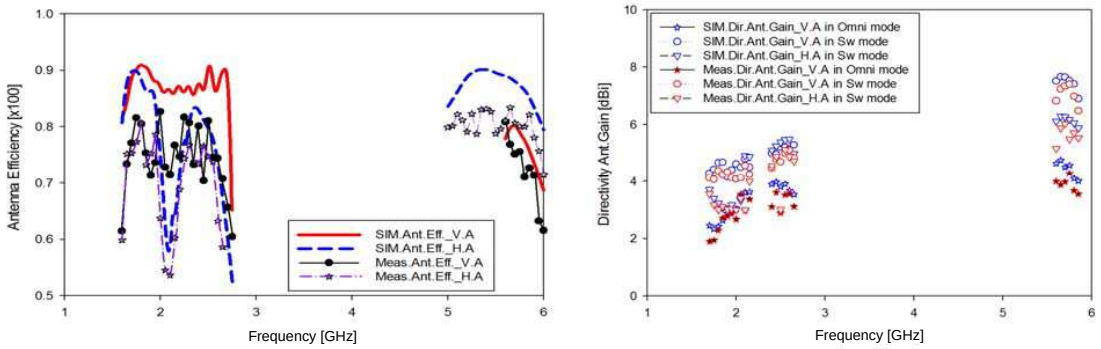

Figure 11. (a) The simulation and measurement antenna efficiency and (b) directivity gain at operation frequencies.

in switched modes for horizontal polarizations, were also investigated. The figures, sequentially from the left to the right side of Figure A5–Figure A8, demonstrate the beam patterns of the H.A, which can be changed by the activation of the specific Sw#i by selecting the H.A#i as an operating element. Figure 11 shows the simulation and measurement antenna efficiency (a) and directivity gain (b) at operation frequencies. At most of operating frequencies of interest, the antenna efficiency is better than 75% for the measurement, and the directivity antenna gain archieves at ∼3 dB, 5 dB for directional modes of V.A at lower bands and higher band, respectively.

4. MIMO PERFORMANCE EVALUATION OF PROPOSED ANTENNA IN DIFFERENT MODES

In order to evaluate the performance of the proposed multiband, dual-polarization, dual-antenna switched beam in a MIMO system, we specially installed a channel capacity measurement system in a reverberation chamber located at KAIST. Then, the MIMO performance and channel capacity were measured at 2.5 GHz and the results are plotted. As discussed earlier, the horizontal antenna could be operated only in switched modes, while the vertical antenna could be worked in two modes, i.e., both omnidirectional and beams-witched modes. As shown in Figure 12, the multiband dual-polarization dual-antenna switched beam antenna system has exhibited a better higher channel capacity when the V.A works in switched beam modes under high signal-to-noise ratio rather than in omni-

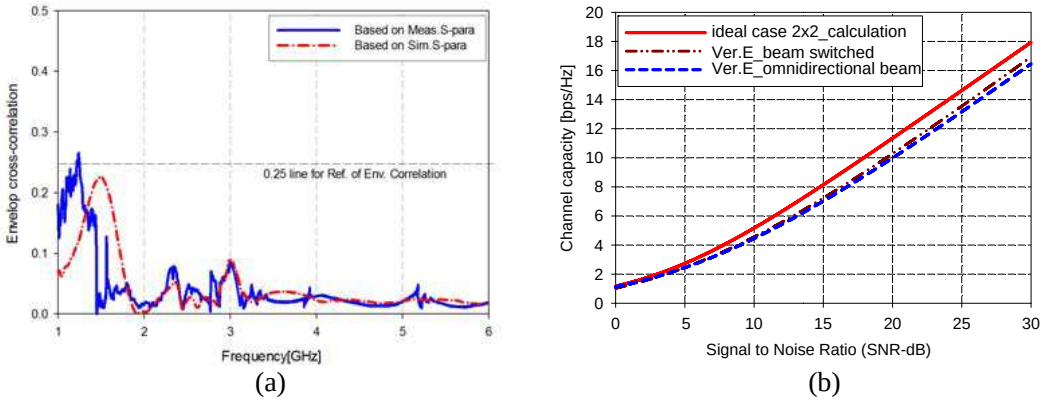

Figure 12. (a) The simulated and measured envelope correlation-coefficent between the two ports dual-polarized, dual-antenna system, (b) the MIMO performance and channel-capacity measurement setup in a reverberation chamber at 2.5 GHz.

directional modes. Space diversity is a well-known technique for improving signal quality in a wireless communication system. In fact, diversity antenna gain is an important factor for the improvement of a diversity antenna system compared with a single-antenna system. Antenna system performance depends on the envelope correlations and power imbalance between the diverted signals [12]. A general form of envelope correlation can be calculated as defined in [13], by using the S-parameters, which is less complex and takes less time than the measurements of the field patterns. Figure 12(a) shows the simulated and measured envelope correlation-coefficient between the proposed two ports dual-polarized, dual-antenna system. If the correlation is high, the received signals may suffer from deep fading simultaneously. According to [14, 15], the criteria $\rho_e < 0.5$ is necessary to obtain an obvious improvement from a diversity system.

5. CONCLUSIONS

In this paper, we have presented a novel multiband, dual-polarization, beam-switched dual-antenna design for small cell base stations that can cover multi-bands, some bands for LTE (1.7–2.1 GHz) and for WLAN (2.5 GHz and 5.8 GHz) applications. The design methodology of the proposed antenna was based on the printed monopoles for both horizontal and vertical antennas. The switching mechanism was adopted by installing p-i-n diode switches on the ports of the dual antennas. The pattern reconfigurability was inspected using an RFSR technique. The RFSR conductive material was square-shaped for pattern steering. Further studies need to be carried out by implementing other shapes for better performance. Noticeably, based on the comparisons of all results including S-parameters and beam patterns of both V.A and H.A, the simulation and measurement results are significantly well matched under a sufficient bandwidth at the target of desired frequencies for LTE and WLAN. Moreover, the design of the proposed antenna seems flexible and easily tunable to other frequency bands, and it is likely to be a cost-effective solution as it can be constructed both with the use of a relatively cheap FR4 substrate and in a simple structure. Furthermore, we have successfully fabricated and measured a prototype of the dual-port multi-band dual-polarization switched beam antenna for indoor base stations in the wireless systems. The investigation of the MIMO performance and channel capacity has clearly demonstrated that this dual-port multi-band dual-polarization switched-beam antenna can be a good candidate for small wireless indoor base stations.

ACKNOWLEDGMENT

This research was financially supported by the National Research Foundation of Korea (NRF) grant funded by the Korea government (MSIP) (NRF-2013R1A2A1A01014518) and by the MSIP (Ministry of Science, ICT & Future Planning), Korea in the ICT R&D Program 2013. (No. 1297204001-130010200).

APPENDIX A.

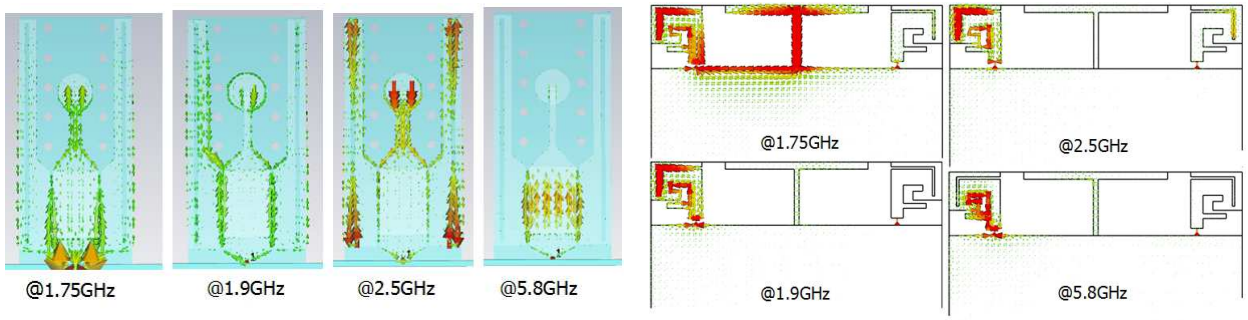

Figure A1. The simulated surface current distributions of (a) the V.A antenna and (b) H.A antenna at different frequencies (1.75 GHz, 1.9 GHz, 2.5 GHz and 5.8 GHz).

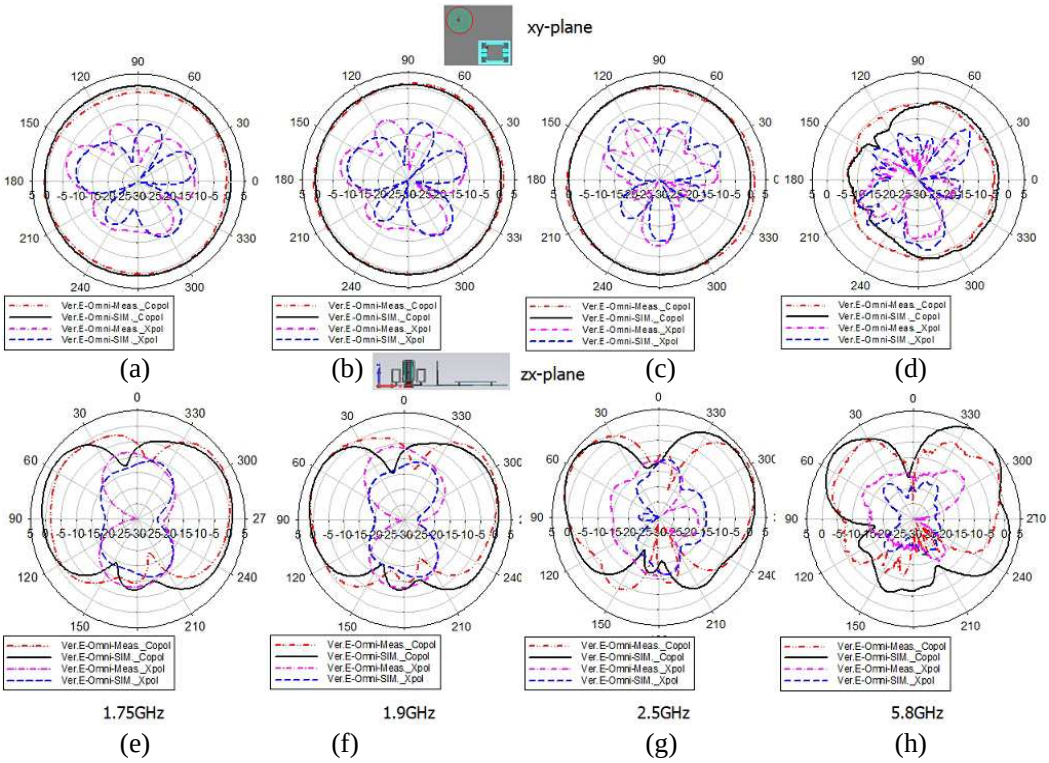

Figure A2. The measured beam patterns of the V.A in omni-directional modes at different frequencies. (a), (b), (c), (d) xy-plane, (e), (f), (g), (h) zx-plane. (a), (e) 1.75 GHz, (b), (f) 1.9 GHz, (c), (g) 2.5 GHz, and (d), (h) 5.8 GHz.

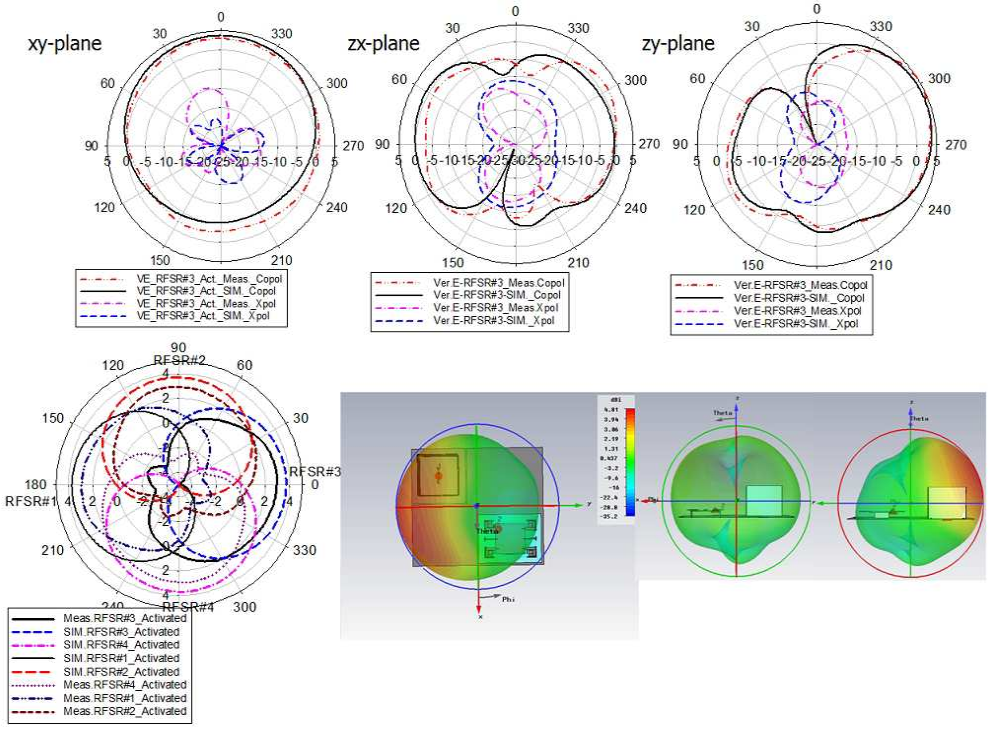

Figure A3. The measured beam patterns of the V.A in switched modes at 1.75 GHz, and at different active RFSR#i.

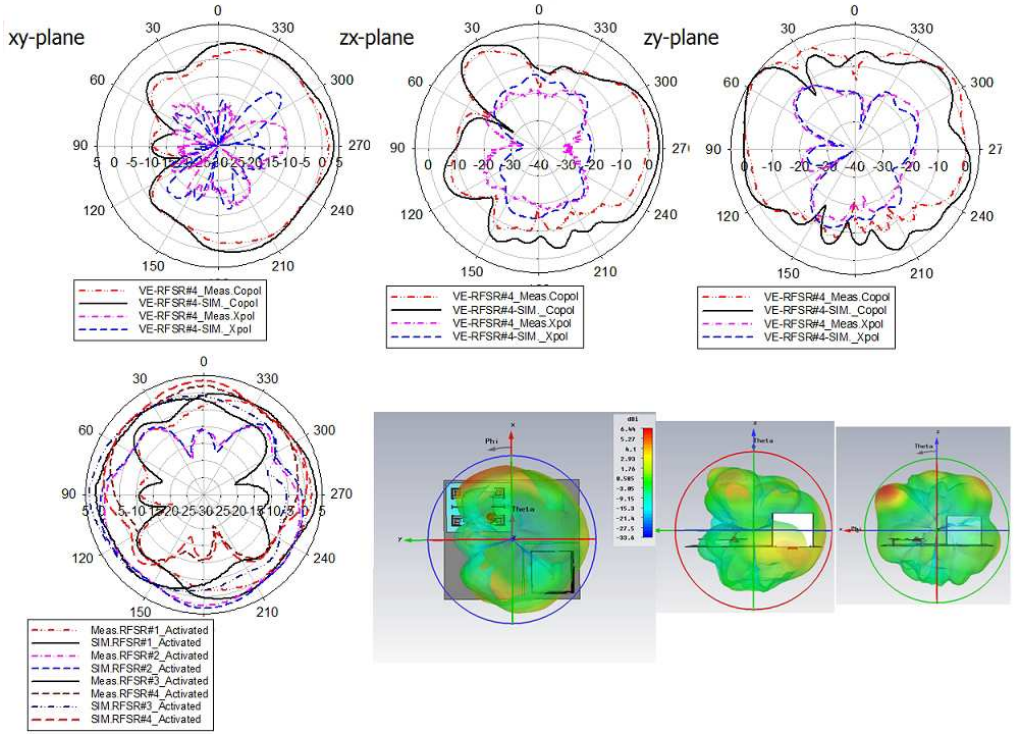

Figure A4. The measured beam patterns of the V.A in switched modes at 5.8 GHz, and at different active RFSR#i.

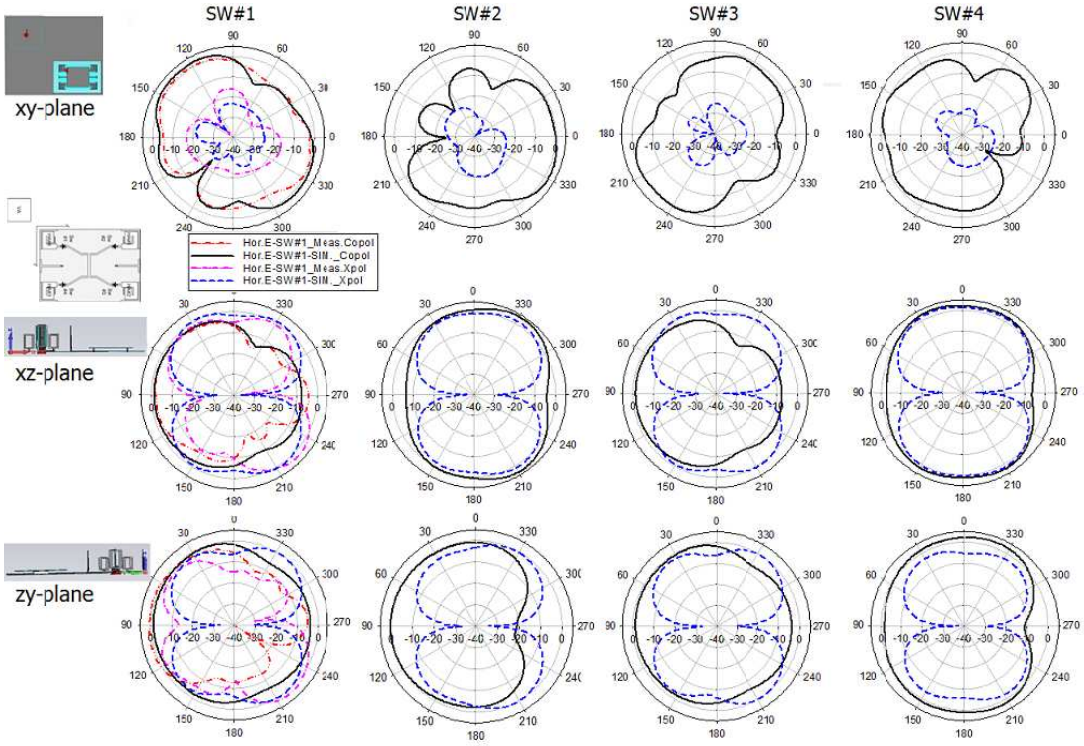

Figure A5. The measured beam patterns of the H.A in switched modes at 1.75 GHz, and at different active SW#i.

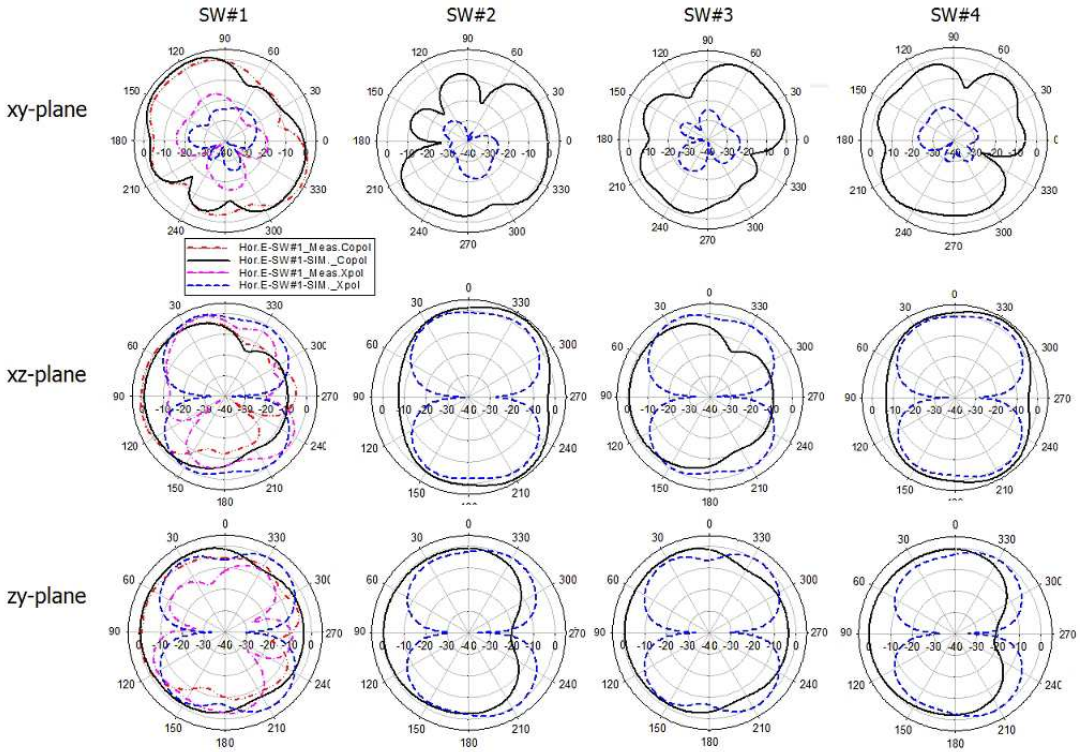

Figure A6. The measured beam patterns of the H.A in switched modes at 1.9 GHz, and at different active RFSR#i.

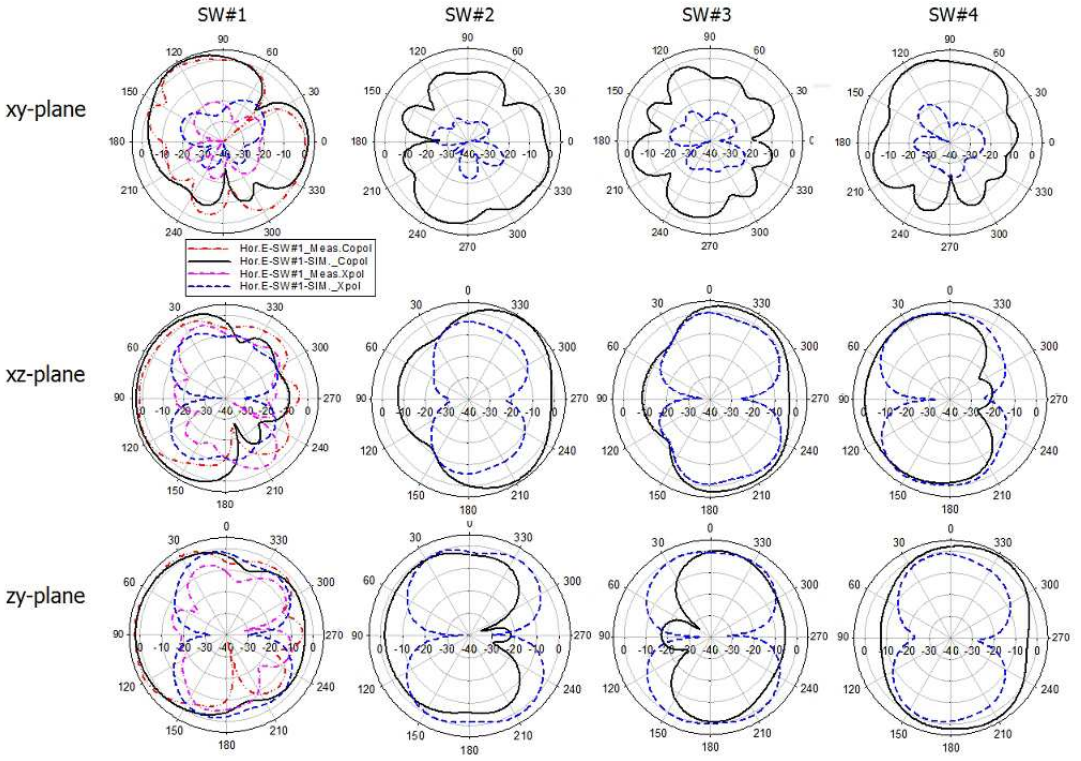

Figure A7. The measured beam patterns of the H.A in switched modes at 2.5 GHz, and at different active SW#i.

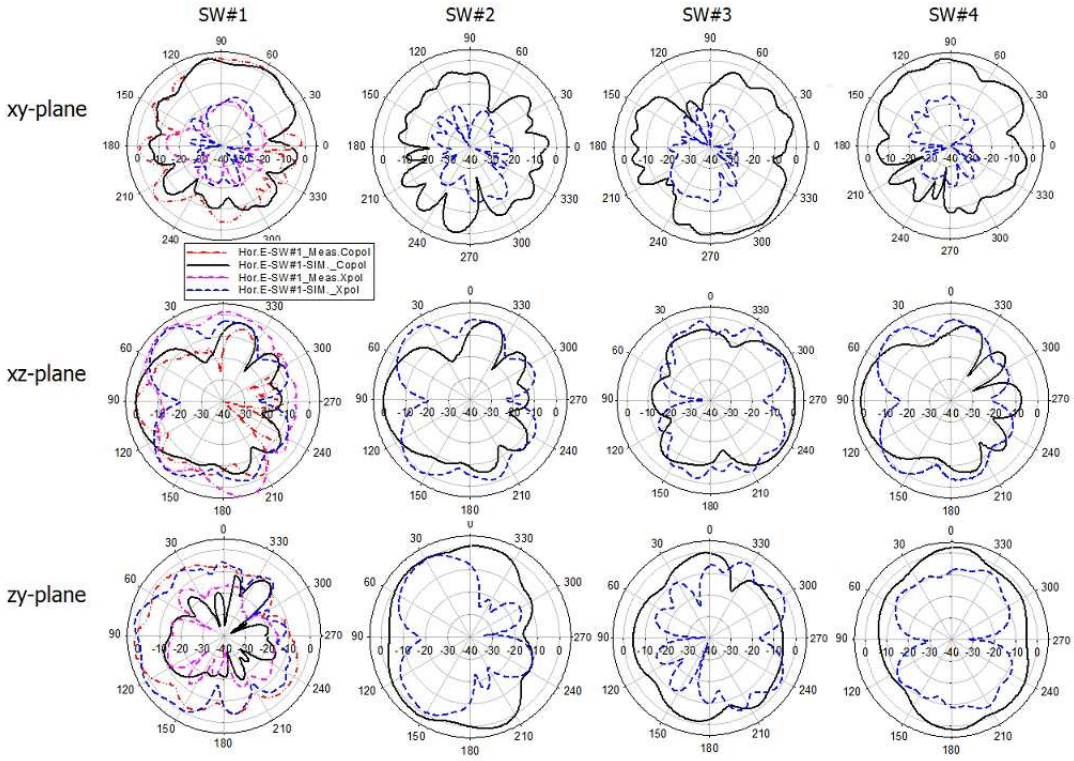

Figure A8. he measured beam patterns of the H.A in switched modes at 5.8 GHz, and at different active RFSR#i.

REFERENCES

1. Matsunaga, M. and T. Matsunaga, "A dual-polarization single-layered antenna for GPS and ISM bands," *IEEE Antennas and Propagation Society International Symposium (APSURSI)*, 1–2, 2012.
2. Ping, S. L., H. Trigui, S. Dean, and Y. Bing, "Low profile multibeam dual polarization antenna array with compensated mutual coupling," *IEEE Antennas and Propagation Society International Symposium (APSURSI)*, 1–2, 2012.
3. Isenlik, T., M. M. Bilgic, K. Yegin, and M. Ciydem, "GSM/UMTS dual polarization base station antenna design," *General Assembly and Scientific Symposium (URSI)*, 1–4, 2011.
4. Bao, Z., Z. Nie, and X. Zong, "A broadband dual-polarization antenna element for wireless communication base station," *IEEE Asia-Pacific Conf. on Antennas and Propagation (APCAP)*, 144–146, 2012.
5. Wang, S., H. Arai, H. Jiang, and K. Cho, "A compact orthogonal dual-polarization combined antenna for indoor MIMO base station," *International Symposium on Antenna Technology and Applied Electromagnetics (ANTEM)*, 1–3, 2012.
6. Liu, X., S. He, H. Zhou, J. Xie, and H. Wang, "A novel low-profile, dual-band, dual-polarization broadband array antenna for 2G/3G base station," *IET International Conference on Wireless, Mobile and Multimedia Networks*, 1–4, 2006.
7. Wu, Z., J. Pan, S. Hu, S. Wen, and D. Yang, "Design of a novel dual polarization wideband base station antenna," *International Symposium on Intelligent Signal Processing and Communication Systems (ISPACS)*, 1–4, 2010.
8. Nguyen, V. A., M. H. Jeong, M. T. Dao, and S. O. Park, "Four-port beam reconfigurable antenna array for pattern diversity system," *IET Microwaves, Antennas & Propagation*, Vol. 6, No. 10, 1179–1186, 2012.
9. Tarn, I. Y. and S. J. Chung, "A novel pattern diversity reflector antenna using reconfigurable

frequency selective reflectors," *IEEE Trans. Ant. & Pro.*, Vol. 57, No. 10, 3035–3042, 2009.

10. Ko, C. H., I. Y. Tarn, and S. J. Chung, "A compact dual-band pattern diversity antenna by dual-band reconfigurable frequency-selective reflectors with a minimum number of switches," *IEEE Trans. Ant. & Pro.*, Vol. 61, No. 2, 646–654, 2013.
11. CST Microwave Studio by Computer Simulation Technology, Online Available: http://www.cst.com.
12. Saunders, S. R., *Antenna and Propagation for Wireless Communication System*, Wiley, New York, 1999.
13. Dossche, S., J. Romeu, and S. Blanch, "Representation of the envelope correlation as a function of distance and frequency for a two-port antenna system," *IEEE Antennas and Propagation Society International Symposium (APSURSI)*, Vol. 2, 1728–1731, 2004.
14. Vaughan, R. G. and J. B. Andersen, "Antenna diversity in mobile communications," *IEEE Trans. Veh. Technol.*, Vol. 36, 149–172, 1987.
15. Karaboikis, M., C. Soras, G. Tsachtsiris, and V. Makios, "Compact dual-printed inverted-F antenna diversity systems for portable wireless devices," *IEEE Antennas Wirel. Propag. Lett.*, Vol. 3, 9–14, 2004.